catalysts

MDPI

Article

An Efficient Electrocatalyst for Oxygen Evolution Reaction in Alkaline Solutions Derived from a Copper Chelate Polymer via In Situ Electrochemical Transformation

Ridwan P. Putra [1], Hideyuki Horino [2] and Izabela I. Rzeznicka [1,*]

[1] Graduate School of Engineering and Science, Shibaura Institute of Technology, Fukasaku 307, Saitama 337-8570, Japan; mg17503@shibaura-it.ac.jp

[2] Department of Chemistry for Materials, Graduate School of Engineering, Mie University, 1577 Kurimamachiya-cho, Mie, Tsu 514-8507, Japan; hideyuki.horino.a6@tohoku.ac.jp

* Correspondence: izabela@shibaura-it.ac.jp; Tel.: +81-48-720-6409

Received: 21 January 2020; Accepted: 12 February 2020; Published: 15 February 2020

Abstract: Efficient oxygen evolution reaction (OER) electrocatalysts are highly desired in the field of water electrolysis and rechargeable metal-air batteries. In this study, a chelate polymer, composed of copper (II) and dithiooxamide, was used to derive an efficient catalytic system for OER. Upon potential sweep in 1 M KOH, copper (II) centers of the chelate polymer were transformed to CuO and $Cu(OH)_2$. The carbon-dispersed CuO nanostructures formed a nanocomposite which exhibits an enhanced catalytic activity for OER in alkaline media. The nanocomposite catalyst has an overpotential of 280 mV (at 1 mA/cm^2) and a Tafel slope of 81 mV/dec in 1M KOH solution. It has a seven-fold higher current than an IrO_2/C electrode, per metal loading. A catalytic cycle is proposed, in which CuO undergoes electrooxidation to Cu_2O_3 that further decomposes to CuO with the release of oxygen. This work reveals a new method to produce an active nanocomposite catalyst for OER in alkaline media using a non-noble metal chelate polymer and a porous carbon. This method can be applied to the synthesis of transition metal oxide nanoparticles used in the preparation of composite electrodes for water electrolyzers and can be used to derive cathode materials for aqueous-type metal-air batteries.

Keywords: electrocatalyst; oxygen evolution reaction; dithiooxamide; chelate polymers; copper oxides; metal–air batteries; alkaline

1. Introduction

The oxygen evolution reaction (OER) is an important half-reaction in the field of electrochemical energy storage and conversion [1–3]. The OER requires a thermodynamic potential of 1.23 V vs. the reversible hydrogen electrode (RHE) and follows different chemical routes depending on pH ($2H_2O \rightarrow 4H^+ + O_2 + 4e^-$ (acidic); $4OH^- \rightarrow O_2 + 2H_2O + 4e^-$ (alkaline)) [4,5]. The development of an efficient, durable and cost-effective electrocatalyst for the OER is required for the advancement of a number of sustainable energy technologies involving water electrolyzers and metal–air batteries.

At present, IrO_2 and RuO_2 are used as catalysts for the OER due to their low overpotential [6]. The high price of Ir and Ru metals, as well as the instability of RuO_2 and IrO_2 at high anodic potentials are major drawbacks that are driving the development of new OER catalysts. Alkaline media offer a greater material choice. Various metal and metal oxide nanoparticles have been tested as OER catalysts in alkaline solutions [3,7,8]. Among transition metals, Co, Fe, Mn, Ni and Cu were frequently investigated. The performance of these catalysts in the OER are frequently summarized in terms of the

overpotential at given current density, though the mass activity (current per metal loading) would be a better descriptor of catalysts efficiency [9,10].

In 2014, Liu et al. showed that nanostructured copper oxide films, deposited from copper (II) complexes on a fluorine-doped tin oxide (FTO) electrode can efficiently catalyze OER in alkaline solutions [11]. The overpotential of the catalyst obtained from copper (II) ethylenediamine complex was estimated to be 475 mV at 10 mA/cm^2. Due to this relatively low overpotential, various copper (II) organic complexes and copper (II) salts were investigated for their activity towards water oxidation. High water oxidation rates were observed for complexes with low electrochemical stability [12]. The enhanced catalytic activity was thus ascribed to CuO particles produced via electrodecomposition of the initial complex. In order to identify catalytically active species, Deng et al. investigated the OER in alkaline solutions on Cu_2O and CuO films, plated on a Cu disk, from solutions containing $CuSO_4$. Cu(III) centers were proposed to be catalytically active species based on the analysis of in situ Raman and X-ray absorption near-edge structure (XANES) results. [5]. These findings motivated researchers to prepare the OER active catalyst by controlling the size, shape and dispersion of copper oxides [13]. Various methods such as hydrothermal, electrochemical and sonochemical can be used to prepare copper oxide nanoparticles [14]. High temperature treatment of CuO films yields particles with the size >200 nm. Such films were found active towards the OER and stable in alkaline solutions, with an overpotential of 430 mV at 1 mA/cm^2 [15]. The drawback of using copper oxides as electrocatalysts is their low electronic conductivity. The general approach to improve the conductivity of oxide electrocatalysts is to mix them with a conductive material such as carbon.

Here, a new method to produce small size CuO nanoparticles, via in situ electrochemical transformation of copper (II) dithioxamide (Cu(dto)) chelate polymer in a carbon matrix, is described. The derived CuO nanocomposite catalyst showed a high catalytic activity towards the OER in alkaline solutions. The use of the chelate polymer was expected to provide a well-dispersed metal templating platform. The catalyst yielded overpotential of only 280 mV at 1 mA/cm^2. To the best of our knowledge, there are no reports that describe potential of chelate polymers in electrocatalysis.

2. Results and Discussion

2.1. Characterization of Cu(dto) Compound

Cu(dto) compound was obtained using several copper salts. The yields obtained from $CuSO_4$, $Cu(NO_3)_2$, $Cu(CH_3COO)_2$ and $CuCl_2$ were 100%, 99%, 94% and 100%, respectively. Figure 1a shows XRD patterns for Cu(dto) compounds prepared from different copper precursors.

All precursors give XRD patterns characterized by two broad peaks at the 2θ value of 15.2° and 28.4°. The shape and position of the peaks are in agreement with the XRD patterns reported in the literature [17]. Figure 1b shows a SEM image of the Cu(dto) compound, obtained from $CuSO_4$. In general, Cu(dto) exists in the form of a very fine powder. An analysis of the energy dispersive X-ray (EDX) results, revealed that copper and dto in the Cu(dto) compound are in 1:1 stoichiometric ratio, as calculated from the atomic ratio of copper to sulfur which was 25.75%:60.58%. The obtained ratio is consistent with the elemental analysis results, and the proposed structure of Cu(dto) compound shown in Figure 1c [16,18].

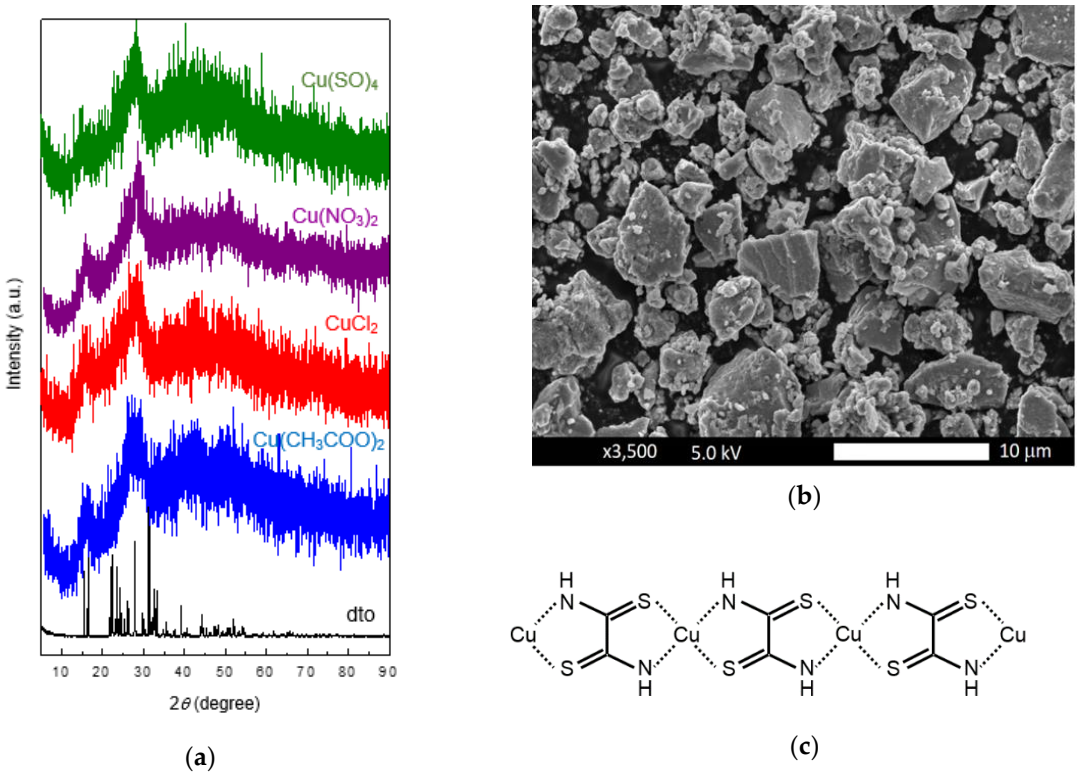

(**a**) (**b**) (**c**)

Figure 1. (**a**) XRD patterns of dto, and Cu(dto) compounds obtained from different copper salts. (**b**) SEM image of Cu(dto) compound obtained from $CuSO_4$ (**c**) proposed polymeric chain structure of Cu(dto) chelate polymer [16].

2.2. Electrochemical Characterization

Cyclic voltammograms (CV) of the Cu(dto) in the first and higher redox cycle are shown in Figure 2. These cyclic voltammograms were taken in 1M KOH and recorded between 0.42 and 1.57 V (vs. RHE) from the open circuit potential at a scan rate of 5 mV/s. In the first cycle, a large anodic peak was observed at 1.18 V vs. RHE. From the second cycle, three anodic peaks at the potential of 0.83 V, 0.91 V and 1.37 V (vs. RHE), and two cathodic peaks at 1.35 V and 0.60 V (vs. RHE) were observed, indicating that the Cu(dto) compound underwent chemical transformations.

In comparison with the CV of a copper foil in 1M KOH solution, the anodic peaks were ascribed to the "$Cu_2O \rightarrow Cu(OH)_2/CuO$", "$Cu(OH) \rightarrow Cu(OH)_2$"' and "$Cu(OH)_2 \rightarrow Cu_2O_3$" alterations, respectively. The two cathodic peaks observed at 1.35 and 0.60 V (vs. RHE) were assigned to the "$Cu_2O_3 \rightarrow Cu(OH)_2$" and "$Cu(OH)_2 \rightarrow Cu_2O$" transitions, respectively [5,19–21]. At a potential around the OER (> 1.5 V vs. RHE), a sharp current increase was observed. The value of the current increase was five-fold in comparison to the glassy carbon electrode (GCE). Bubbles emerging from the electrode surface were clearly visible at the onset of the OER [5].

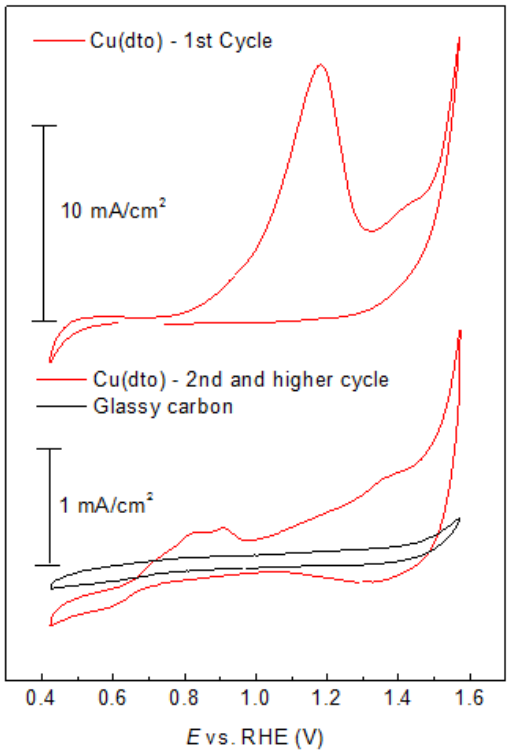

Figure 2. Cyclic voltammograms of the Cu(dto)/C electrode and a glassy carbon electrode at a scan rate of 5 mV/s, in N_2-saturated 1 M KOH.

2.3. Electrocatalytic Characterization

The OER performance of Cu(dto)/C electrode was further compared with the performance of IrO_2/C, CuO/C and Cu bare electrode in 1 M KOH using the linear sweep voltammetry (LSV) technique. The results are shown in Figure 3a,b. Before taking LSV, the Cu(dto)/C electrode was subject to 130 potential cycles, as described in the experimental part. At a current density of 10 mA/cm^2, the Cu(dto)/C electrode showed an overpotential of 400 mV. Neither the IrO_2/C nor the Cu bare electrode reached a current density of 10 mA/cm^2 within the measured potential window, therefore the overpotential for all the samples was evaluated at 1 mA/cm^2.

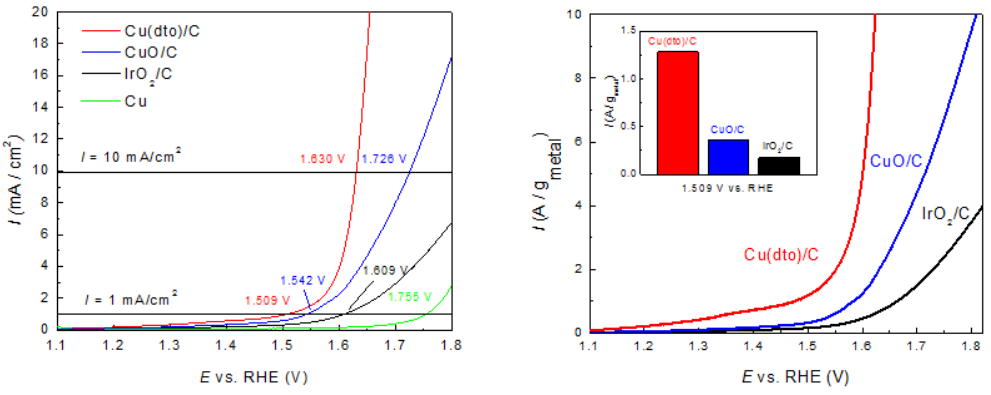

Figure 3. Linear sweep voltammetry (LSV) curves at a scan rate of 5 mV/s, conducted in N_2-saturated 1 M KOH. (**a**) in the current per electrode surface area. (**b**) in the current per gram of the active metal. In the inset, the mass activity at 1.509 V is compared.

The results show that the Cu(dto)/C electrode exhibits the lowest OER overpotential of 279 mV at 1 mA/cm^2. The overpotential for IrO_2/C, CuO/C and the Cu bare electrode, obtained under identical conditions, was 379, 312 and 525 mV, respectively. The overpotential for IrO_2/C in 1M KOH is slightly higher than reported. The difference is likely due to different IrO_2 nanoparticle synthesis protocols or the nature of the carbon matrix [22,23]. Here, commercially available materials were used for ease of inter laboratory comparison. The performance of the Cu(dto)/C electrode is superior to other copper-based OER catalysts in terms of overpotential at a current density of 10 mA/cm^2. The overpotential in 1M KOH is 475 mV for Cu-ethylenediamine (EA) derived CuO [11], 340 mV for Cu@CuO-C hybrid nanorods [24], 350 mV for Cu_2O-Cu core-shell nanorods [25], 400 mV for $CuCo_2O_4$-SSM phase-pure spinel [26] and 410 mV for $CuRhO_2$ delafossite [27]. Moreover, the Cu(dto) electrode showed a significantly lower OER overpotential at a current density of 10 mA/cm^2 compared to a commercial CuO/C system composed of nanoparticles with an average size of 50 nm (400 mV vs. 496 mV). The result indicates that in situ electrochemical oxidation of Cu(dto) chelate polymer leads to small and well-dispersed CuO nanostructures, which significantly enhance the OER catalytic activity. The mass activity was further compared. Figure 3b shows LSV plots for Cu(dto)/C, CuO/C and IrO_2/C electrodes, in terms of current per gram of a metal contained in the slurry deposited on the electrode. It can be seen that the Cu(dto) electrode has a seven-fold higher current than IrO_2/C electrode.

The Cu(dto)/C electrode also has a small Tafel slope value of 81 mV/dec, as shown in Figure 4. Under the same conditions, the CuO/C electrode has a slope of 160 mV/dec and the Cu bare electrode a slope of 271 mV/dec. IrO_2/C has a Tafel slope of 189 mV/dec. This implies that the Cu(dto)/C electrode has the most favorable OER kinetic performance among all tested materials. Its catalytic performance is comparable to other non-noble metal catalysts such as metallic Co_2N (80 mV/dec) [28], $La_{0.2}Sr_{0.8}Fe_{0.2}Co_{0.8}O_3$ perovskite (80 mV/dec) [29], Ni foam /N-CNTs/$Ni(OH)_2$ nanosheets (84 mV/dec) [30] and NiS microsphere foam (89 mV/dec) [31]. Table 1 summarizes the OER performance of the materials evaluated in the present study.

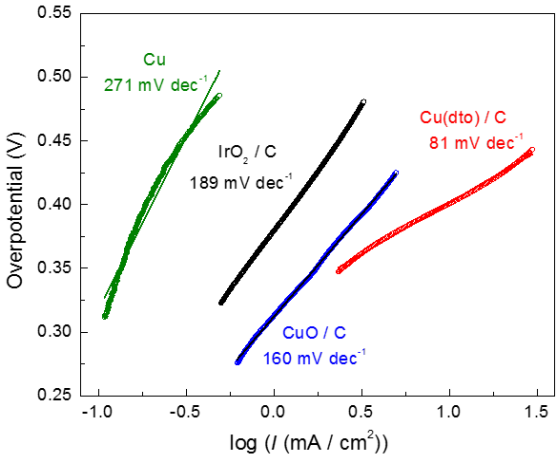

Figure 4. Tafel plots for all tested electrodes.

Table 1. Summary of oxygen evolution reaction (OER) performance of the tested materials in N_2-saturated 1 M KOH.

Catalysts	η (mV) at J = 1 mA cm^{-2}	E_{OER} (V) [a] at J = 1 mA cm^{-2}	η (mV) at J = 10 mA cm^{-2}	E_{OER} (V) [a] at J = 10 mA cm^{-2}	Tafel Slope (mV dec^{-1})
Cu(dto)/C	279	1.509	400	1.630	81
CuO/C	312	1.542	496	1.726	160
IrO_2/C	379	1.609	-	-	189
Cu	525	1.755	-	-	271

[a] All potential values are reported vs. the reversible hydrogen electrode (RHE).

2.4. Surface Morphology and Composition after Electrochemical Cycling

In order to understand the chemical transformation which took place during electrochemical cycling, XRD was taken both before and after CV measurements. The electrode was subjected to 130 cycles in 1M KOH. Figure 5 shows the XRD patterns of the pre-cycling and post-cycling electrodes. Analysis of the XRD spectra indicates that the Cu(dto) compound was transformed into CuO and Cu_2O upon potential cycling [32,33]. Corresponding XRD patterns are in good agreement with the JCPDS No. 48-1548 and 05-0667 spectra, which refer to CuO and Cu_2O, respectively. After the formation of copper oxides, the broad peaks observed at the 2θ values of 15.2° and 28.4° (which are characteristic of the Cu(dto) compound) disappeared, leaving only a single broad peak in the range of 2θ between 10° and 30°, which are due to acetylene black present in the slurry. The average CuO particle size was estimated using the Scherrer formula. A value of 39 nm was obtained from the peak at 2θ of 35°, corresponding to the (111) facet of CuO. Independent measurements using TEM taken on post-cycled powder reveal the presence of particles with a size between 10–50 nm and modus size of 25 nm (Figure S2).

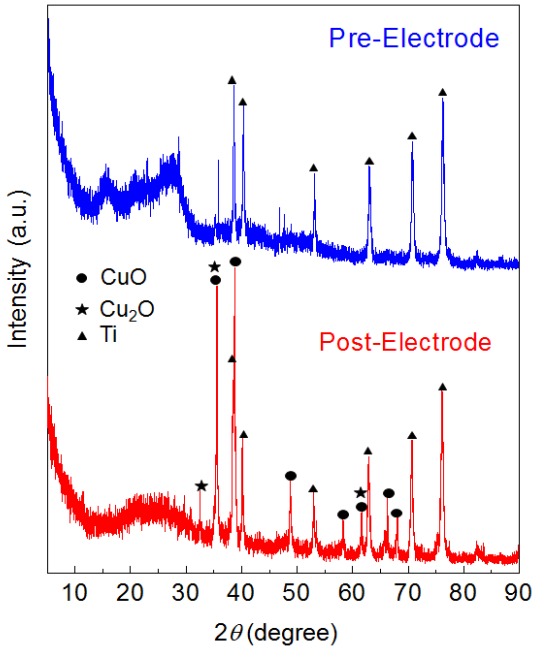

Figure 5. XRD patterns of pre- and post-cycling electrodes, taken on a titanium foil.

SEM images of the pre- and post-cycling electrodes are shown in Figure 6a–c respectively. The SEM image of the electrode after the cycling shows grain-like nanostructures with well distributed flower-like objects (Figure 6c).

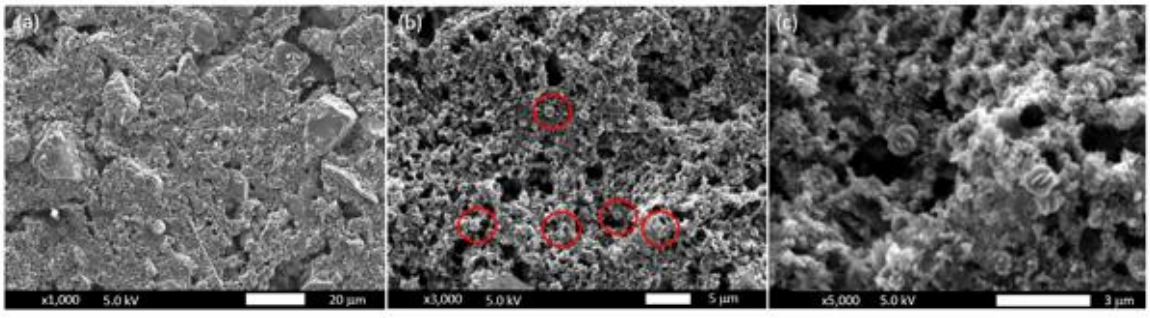

Figure 6. SEM images of (**a**) the pre-cycling electrode and (**b**,**c**) the post-cycling electrode.

It can also be noticed that the material became more porous with many holes through which gas diffused into the electrolyte solution. From the areal EDX measurements, it was found that the atomic ratio of Cu:O in the flower-like structures and grain-like structures was 33.5%:15.92% (1:2) and 0.82%:1.17% (2:1), respectively. Thus, we concluded that the areas with flower-like structures are mostly populated by Cu_2O species and the areas with small grain-like structures correspond to CuO species. These Cu(dto)-derived oxides, (Cu(dto)-DO—'DO' is used to designate the dithiooxamide-derived oxide from here on) are in fact the active OER electrocatalyst. Similar findings were recently reported using a copper-ethylene diamine (CuEA) compound to derive copper oxides [11]. Only a small amount of sulfur was found in the post-cycling electrodes. The atomic ratio of Cu:S after electrochemical cycling was found to be 33.5%:0.03%, based on EDX analysis. A loss of selenium was also reported in the in situ growth of nickel iron hydroxide from a $Ni_xFe_{1-x}Se_2$ compound. After cycling, only $Ni_xFe_{1-x}(OH)_{3-x}$ species were present and these species were indicated to have catalytic OER activity [34].

2.5. Proposed Catalytic Cycle

In this Cu(dto)-DO electrocatalyst, CuO is proposed to be the active catalytic species for OER. The OER mechanism on the catalyst is initiated by the formation of CuO from Cu(dto) in the first potential sweep according to chemical Equations (1) and (2). Subsequently, CuO will form Cu_2O_3 by the reaction with OH^- present in the electrolyte solution, according to Reaction (3). Finally, Cu_2O_3, as an intermediate species, will release O_2 to reform CuO (Equation (4)). The corresponding chemical reactions are as follows:

$$Cu(dto) \rightarrow Cu^{2+} + dto^{2-} \quad (1)$$

$$Cu^{2+} + 2OH^- \rightarrow CuO + H_2O \quad (2)$$

$$4CuO + 2OH^- \rightarrow 2Cu_2O_3 + 4e^- + 2H^+ \quad (3)$$

$$2Cu_2O_3 \rightarrow 4CuO + O_2 \quad (4)$$

The OER mechanism involving Cu_2O_3 as an intermediate species is proposed based on recent reports in which Cu(III) formation was detected by the UV-VIS method during amperometric measurements [12]. In another study, using in situ Raman spectroscopy, a peak at 603 cm^{-1} was observed at the potential at which OER commences. The peak was assigned to Cu(III) [5]. According to Equations (1)–(4), it is proposed here that the enhanced catalytic activity is due to CuO. Scheme 1 summarizes a possible mechanism leading to oxygen evolution. In this mechanism, Cu_2O_3 is an intermediate species that yields O_2 while recovering CuO.

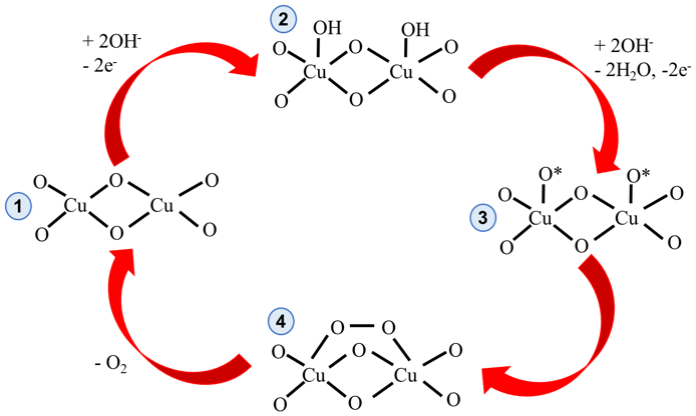

Scheme 1. Proposed mechanism of OER on Cu(dto)-dithiooxamide-derived oxide (DO)/C catalyst in alkaline media.

3. Materials and Methods

3.1. Materials

Copper (II) sulfate ($CuSO_4$, >99%), copper (II) nitrate hydrate ($Cu(NO_3)_2$ *x* H_2O, 99.999%), copper chloride dihydrate ($CuCl_2{\cdot}2H_2O$, 99%), copper (II) oxide nanopowder (50 nm particle size, 29 m^2/g, battery manufacturing grade), N-methyl-2-pyrrolidine (NMP, 99.5%), ferrocenemethanol ($FcCH_2OH$, 97%) and potassium chloride (KCl, >99.99%) were purchased from Sigma Aldrich, St. Louis, MO, USA. Polyvinylidene fluoride (PVDF) was purchased from Kureha Co., Osaka, Japan. Acetylene black (99.99%) was purchased from Strem Chemicals, Inc., Newburyport, MA, USA. Copper (II) acetate ($Cu(CH_3COO)_2$, >97%), dithiooxamide, (dto) ($C_2H_4N_2S_2$, 98%), ethanol (C_2H_5OH, 99.5%), iridium (IV) oxide (IrO_2, >85% (w/w) of Ir) and potassium hydroxide (KOH, >85%) were purchased from FUJIFIM Wako Pure Chemicals Co., Saitama, Japan. All chemicals were used as received without further purification. Deionized water with a specific resistance of 18.2 MΩ and with a total organic carbon (TOC) value below 4 ppm was used throughout the experiments. A glassy carbon electrode (GCE) with a diameter of 3 mm, an Ag/AgCl reference electrode and a platinum rod for a counter electrode were purchased from EC Frontier Inc., Kyoto, Japan. A copper electrode with an inner diameter of 3 mm was purchased from ALS Co., Tokyo, Japan. Titanium foil with a thickness of 0.05 mm was purchased from Nilaco Co., Ltd., Tokyo, Japan.

3.2. Synthesis of Copper Dithiooxamide Cu(dto) Compound

A Cu(dto) compound was synthesized by a co-precipitation method using an aqueous solution of a copper precursor and ethanolic solution of dto in a 1:1 stoichiometric ratio [16]. Several copper precursors were investigated to prepare this compound, including copper sulfate ($CuSO_4$), copper nitrate ($Cu(NO_3)_2$), copper acetate ($Cu(CH_3COO)_2$) and copper chloride ($CuCl_2$). To synthesize the compound, an aqueous solution of a copper precursor was added dropwise into an ethanolic solution of dto at room temperature while stirring the mixture at 200 rpm for 1 h. Black, fine particles, suspended in the solution, were formed immediately after adding a corresponding copper precursor solution. After leaving the solution for 12 h, a dark grey precipitate was present at the bottom of the vial. This precipitate was filtered using a 0.45 μm pore size membrane filter, washed by deionized water several times and dried in vacuo at 80 °C.

3.3. Materials Characterization

Powder X-ray diffraction (XRD) was obtained on a SmartLab Rigaku (Rigaku Co., Ltd., Tokyo, Japan) diffractometer using CuK_α radiation at 1.5406 Å. Scanning electron microscopy (SEM) images and energy dispersive X-ray (EDX) spectra were taken by a FE-SEM7100F with EDX detector (JEOL/JSM-7100F, JEOL Ltd., Tokyo, Japan).

3.4. Catalyst Slurry and Electrode Preparation

Powders of Cu(dto), IrO_2, CuO and acetylene black were mixed in a ratio of 8:1 (w/w) to prepare the Cu(dto)/C, IrO_2/C and CuO/C slurry. PVDF binder was dissolved in an NMP solvent to form a 2% (w/w) solution. This solution was added to the powder mixture, keeping the proportion of PVDF to acetylene carbon in a 1:1 mass ratio. The mixture was then stirred at 1500 rpm for 2 h to form a homogeneous slurry. The surface of the GCE (3 mm inner diameter) was coated by 1 μl of the slurry and dried in vacuo. The slurry-coated electrode was used as a working electrode. The average amount of copper in 1 μl of the slurry was 5.70×10^{-5} g (5.40×10^{17} Cu atoms). A piece of the titanium foil coated by the thin film of slurry was used as the working electrode and used for characterization of the pre- and post-cycling electrodes by XRD and SEM-EDX analysis.

3.5. Electrochemical Tests

The electrochemical tests were performed in a three-electrode system in an aqueous alkaline solution using an automatic polarization system (HZ-7000, Hokuto Denko Co., Tokyo, Japan) under nitrogen saturated conditions without *iR* compensation. An Ag/AgCl (sat'd KCl) electrode and a platinum rod were used as the reference electrode and the counter electrode, respectively. The usage of Pt as a counter electrode did not affect the catalytic performance as no dissolution of Pt occurred. This was confirmed by EDX analysis of the post-cycling electrode [35]. All values of the current density are normalized with respect to the geometrical area of the electrode, which was 0.071 cm^2 for both the GCE and the Cu electrode. Cyclic voltammetry (CV) measurements were performed in the potential window of 0.42–1.57 V vs. RHE with a scan rate of 5 mV/s. To transform the Cu(dto) compound into corresponding copper oxides, the working electrode was subject to around 130 cycles, in the potential range of 0.4–1.6 V (vs. RHE), performed in nitrogen-saturated 1 M KOH solution. The OER performance was investigated using linear sweep voltammetry (LSV) with a scan rate of 5 mV/s. The overpotential refers to the difference between the measured potential at a given current density (1 mA/cm^2 or 10 mA/cm^2) and the standard thermodynamic potential for the OER (1.23 V vs RHE).

Before performing all electrochemical tests, the Ag/AgCl reference electrode was calibrated using 1 mM of ferrocenemethanol in 0.1 M aqueous KCl solution. In this paper, the potential measured using the Ag/AgCl reference electrode was converted to the reversible hydrogen electrode (RHE) potential using the Nernst equation, as follows:

$$E_{RHE} = E_{Ag/AgCl} + 0.059pH + 0.197 \quad (5)$$

4. Conclusions

In summary, an efficient electrocatalytic system for the OER in alkaline solutions has been developed by the in situ electrochemical oxidation of Cu(dto) chelate polymer in a carbon matrix. This catalytic system showed a low OER overpotential and a small Tafel slope, which outperforms the widely used IrO_2/C catalyst in terms of overpotential and current obtained per metal loading. A detailed insight is provided into the transformation of Cu(dto) into the active CuO/C nanocomposite catalyst. A catalytic cycle is proposed in which CuO undergoes electrooxidation to Cu_2O_3 that further decomposes to CuO with releasing oxygen.

The described method of in situ electrochemical transformation of a copper chelate polymer template into the active OER catalyst provides a new method for the preparation of active non-noble metal oxide electrocatalysts for the OER in alkaline solutions. This methodology may find application in the preparation of noble-metal free catalysts for water electrolyzers and aqueous metal-air batteries that operate under alkaline conditions. It has a potential to reduce the cost of the catalyst by replacing usage of noble metals.

Supplementary Materials: The following are available online at http://www.mdpi.com/2073-4344/10/2/233/s1, Figure S1: Cyclic voltammograms of the Cu electrode and Cu(dto)/C electrode at a scan rate of 5 mV/s, in N_2-saturated 1M KOH, Figure S2: TEM image of Cu(dto)-DO/C powder after cycling in the potential window of 0.42–1.57 V vs. RHE with a scan rate of 5 mV/s. TEM image was taken on JEOL 2100 microscope at 200 keV. The powder was deposited from ethanolic solution on a Cu grid (300 mesh) coated with the Lacey Carbon, Table S1: Assignment of the redox reactions in the cyclic voltammograms of the Cu electrode at a scan rate of 5 mV/s, in N_2-saturated 1M KOH.

Author Contributions: The manuscript was written through contributions of all authors. All authors have given approval to the final version of the manuscript. Conceptualization, H.H.; methodology, H.H.; R.P.P.; I.I.R.; experiments, R.P.P.; analysis, R.P.P.; writing—original draft preparation, R.P.P.; writing—review and editing, R.P.P.; H.H.; I.I.R.; funding acquisition, I.I.R.

Funding: This research received no external funding.

Acknowledgments: The author R.P.P. thanks Japan International Cooperation Agency (JICA) through Innovative Asia Program scholarship for financial support. I.I.R. thanks Shibaura Institute of Technology and JICA for

financial supports. The authors express their thanks to the N. Imanishi's group at Mie University and A. Yamamoto group at Shibaura Institute of Technology.

Conflicts of Interest: The authors declare no conflicts of interest.

References

1. Tahir, M.; Pan, L.; Idrees, F.; Zhang, X.; Wang, L.; Zou, J.-J.; Wang, Z.L. Electrocatalytic Oxygen Evolution Reaction for Energy Conversion and Storage: A Comprehensive Review. *Nano Energy* **2017**, *37*, 136–157. [CrossRef]
2. Park, S.; Shao, Y.; Liu, J.; Wang, Y. Oxygen Electrocatalysts for Water Electrolyzers and Reversible Fuel Cells: Status and Perspective. *Energy Environ. Sci.* **2012**, *5*, 9331–9344. [CrossRef]
3. Wang, Z.-L.; Xu, D.; Xu, J.-J.; Zhang, X.-B. Oxygen Electrocatalysts in Metal-air Batteries: From Aqueous to Nonaqueous Electrolytes. *Chem. Soc. Rev.* **2014**, *43*, 7746–7786. [CrossRef] [PubMed]
4. Kondo, M.; Masaoka, S. Water Oxidation Catalysts Constructed by Biorelevant First-row Metal Complexes. *Chem. Lett.* **2016**, *45*, 1220–1231. [CrossRef]
5. Deng, Y.; Handoko, A.D.; Du, Y.; Xi, S.; Yeo, B.S. In Situ Raman Spectroscopy of Copper and Copper Oxide Surfaces during Electrochemical Oxygen Evolution Reaction: Identification of CuIII Oxides as Catalytically Active Species. *ACS Catal.* **2016**, *6*, 2473–2481. [CrossRef]
6. Lee, Y.; Suntivich, J.; May, K.J.; Perry, E.E.; Shao-Horn, Y. Synthesis and Activities of Rutile IrO_2 and RuO_2 Nanoparticles for Oxygen Evolution in Acid and Alkaline Solutions. *J. Phys. Chem. Lett.* **2012**, *3*, 399–404. [CrossRef]
7. Reier, T.; Oezaslan, M.; Strasser, P. Electrocatalytic Oxygen Evolution Reaction (OER) on Ru, Ir, and Pt Catalysts: A Comparative Study of Nanoparticles and Bulk Materials. *ACS Catal.* **2012**, *2*, 1765–1772. [CrossRef]
8. Song, F.; Bai, L.; Moysiadou, A.; Lee, S.; Hu, C.; Liardet, L.; Hu, X. Transition Metal Oxides as Electrocatalysts for the Oxygen Evolution Reaction in Alkaline Solutions: An Application-Inspired Renaissance. *J. Am. Chem. Soc.* **2018**, *140*, 7748–7759. [CrossRef]
9. McCrory, C.C.L.; Jung, S.; Peters, J.C.; Jaramillo, T.F. Benchmarking Heterogeneous Electrocatalysts for the Oxygen Evolution Reaction. *J. Am. Chem. Soc.* **2013**, *135*, 16977–16987. [CrossRef]
10. Eftekhari, A. Tuning the Electrocatalysts for Oxygen Evolution Reaction. *Mater. Today Energy* **2017**, *5*, 37–57. [CrossRef]
11. Liu, X.; Cui, S.; Qian, M.; Sun, Z.; Du, P. In Situ Generated Highly Active Copper Oxide Catalysts for the Oxygen Evolution Reaction at Low Overpotential in Akaline Solutions. *Chem. Commun.* **2016**, *52*, 5546–5549. [CrossRef]
12. Najafpour, M.M.; Mehrabani, S.; Mousazade, Y.; Hołyńska, M. Water Oxidation by A Copper(II) Complex: New Findings, Questions, Challenges and A New Hypothesis. *Dalton Trans.* **2018**, *47*, 9021–9029. [CrossRef]
13. Liu, X.; Cui, S.; Sun, Z.; Du, P. Copper Oxide Nanomaterials Synthesized from simple Copper Salts as active Catalysts for Electrocatalytic Water Oxidation. *Electrochim. Acta* **2015**, *160*, 202–208. [CrossRef]
14. Silva, N.; Ramírez, S.; Díaz, I.; Garcia, A.; Hassan, N. Easy, Quick, and Reproducible Sonochemical Synthesis of CuO Nanoparticles. *Materials* **2019**, *12*, 804. [CrossRef]
15. Liu, X.; Cui, S.; Sun, Z.; Ren, Y.; Zhang, X.; Du, P. Self-Supported Copper Oxide Electrocatalyst for Water Oxidation at Low Overpotential and Confirmation of Its Robustness by Cu K-Edge X-ray Absorption Spectroscopy. *J. Phys. Chem. C* **2016**, *120*, 831–840. [CrossRef]
16. Abboudi, M.; Mosset, A.; Galy, J. Metal Complexes of Rubeanic Acid. Large-angle X-ray Scattering Studies of Amorphous Copper(II) and Nickel(II) Complexes. *Inorg. Chem.* **1985**, *24*, 2091–2094. [CrossRef]
17. Kanda, S.; Ito, K.; Nogaito, T. Magnetic and Electrical Properties of Coordination Polymers Formed with Copper and Rubeanic Acid. *J. Polym. Sci. Polym. Symp.* **1967**, *17*, 151–162. [CrossRef]
18. Kanda, S.; Suzuki, A.; Ohkawa, K. Syntheses of Nonstereospecific and Stereospecific Lamellar Coordination Polymers. N,N -Disubstituted Dithiooxamides Copper Coordination Polymers. *Ind. Eng. Chem. Prod. Res. Develop.* **1973**, *12*, 88–96. [CrossRef]
19. Ambrose, J.; Barradas, R.G.; Shoesmith, D.W. Investigations of Copper in Aqueous Alkaline Solutions by Cyclic Voltammetry. *J. Electroanal. Chem. Interfacial Electrochem.* **1973**, *47*, 47–64. [CrossRef]

20. El Din, A.M.S.; El Wahab, F.M.A. The Behaviour of the Copper Electrode in Alkaline Solutions upon Alternate Anodic and Cathodic Polarization. *Electrochim. Acta* **1964**, *9*, 113–121. [CrossRef]
21. Abd el Haleem, S.M.; Ateya, B.G. Cyclic Voltammetry of Copper in Sodium Hydroxide Solutions. *J. Electroanal. Chem. Interfacial Electrochem.* **1981**, *117*, 309–319. [CrossRef]
22. Zhu, Y.P.; Jing, Y.; Vasileff, A.; Heine, T.; Qiao, S.-Z. 3D Synergistically Active Carbon Nanofibers for Improved Oxygen Evolution. *Adv. Energy Mater.* **2017**, *7*, 1602928. [CrossRef]
23. Hara, M.; Waraksa, C.C.; Lean, J.T.; Lewis, B.A.; Mallouk, T.E. Photocatalytic Water Oxidation in a Buffered Tris(2,2′-bipyridyl)ruthenium Complex-Colloidal IrO_2 System. *J. Phys. Chem. A* **2000**, *104*, 5275–5280. [CrossRef]
24. Wu, J.-X.; He, C.-T.; Li, G.-R.; Zhang, J.-P. An Inorganic-MOF-inorganic Approach to Ultrathin CuO Decorated Cu–C Hybrid Nanorod Arrays for an Efficient Oxygen Evolution Reaction. *J. Mater. Chem. A* **2018**, *6*, 19176–19181. [CrossRef]
25. Xu, H.; Feng, J.-X.; Tong, Y.-X.; Li, G.-R. Cu_2O–Cu Hybrid Foams as High-Performance Electrocatalysts for Oxygen Evolution Reaction in Alkaline Media. *ACS Catal.* **2017**, *7*, 986–991. [CrossRef]
26. Serov, A.; Andersen, N.I.; Roy, A.J.; Matanovic, I.; Artyushkova, K.; Atanassov, P. $CuCo_2O_4$ ORR/OER Bi-functional Catalyst: Influence of Synthetic Approach on Performance. *J. Electrochem. Soc.* **2015**, *162*, F449–F454. [CrossRef]
27. Hinogami, R.; Toyoda, K.; Aizawa, M.; Kawasaki, T.; Gyoten, H. Copper Delafossite Anode for Water Electrolysis. *ECS Trans.* **2013**, *58*, 27–31. [CrossRef]
28. Chen, P.; Xu, K.; Tong, Y.; Li, X.; Tao, S.; Fang, Z.; Chu, W.; Wu, X.; Wu, C. Cobalt Nitrides as A Class of Metallic Electrocatalysts for the Oxygen Evolution Reaction. *Inorg. Chem. Front.* **2016**, *3*, 236–242. [CrossRef]
29. Matsumoto, Y.; Yamada, S.; Nishida, T.; Sato, E. Oxygen Evolution on $La_{1-x}Sr_xFe_{1-y}Co_yO_3$ Series Oxides. *J. Electrochem. Soc.* **1980**, *127*, 2360–2364. [CrossRef]
30. Wu, J.; Subramaniam, J.; Liu, Y.; Geng, D.; Meng, X. Facile Assembly of $Ni(OH)_2$ Nanosheets on Nitrogen-doped Carbon Nanotubes Network as High-performance Electrocatalyst for Oxygen Evolution Reaction. *J. Alloys Compd.* **2018**, *731*, 766–773. [CrossRef]
31. Zhu, W.; Yue, X.; Zhang, W.; Yu, S.; Zhang, Y.; Wang, J.; Wang, J. Nickel Sulfide Microsphere Film on Ni foam as An Efficient Bifunctional Electrocatalyst for Overall Water Splitting. *Chem. Commun.* **2016**, *52*, 1486–1489. [CrossRef] [PubMed]
32. Meghana, S.; Kabra, P.; Chakraborty, S.; Padmavathy, N. Understanding the Pathway of Antibacterial Activity of Copper Oxide Nanoparticles. *RSC Adv.* **2015**, *5*, 12293–12299. [CrossRef]
33. Yang, Y.; Xu, D.; Wu, Q.; Diao, P. Cu_2O/CuO Bilayered Composite as a High-Efficiency Photocathode for Photoelectrochemical Hydrogen Evolution Reaction. *Sci. Rep.* **2016**, *6*, 35158. [CrossRef]
34. Xu, X.; Song, F.; Hu, X. A Nickel Iron Diselenide-derived Efficient Oxygen-evolution Catalyst. *Nat. Commun.* **2016**, *7*, 12324. [CrossRef] [PubMed]
35. Chen, J.G.; Jones, C.W.; Linic, S.; Stamenkovic, V.R. Best Practices in Pursuit of Topics in Heterogeneous Electrocatalysis. *ACS Catal.* **2017**, *7*, 6392–6393. [CrossRef]

© 2020 by the authors. Licensee MDPI, Basel, Switzerland. This article is an open access article distributed under the terms and conditions of the Creative Commons Attribution (CC BY) license (http://creativecommons.org/licenses/by/4.0/).